Experimental and simulation validation and characterisation of flexural modes in unimorph ultrasound transducers

T.J.R. Eriksson, S.N. Ramadas and S.M. Dixon
University of Warwick, UK
Email: t.j.r.eriksson@warwick.ac.uk

***Abstract*— Two unimorph flexural transducer designs are proposed and tested with regard to mode shapes and frequencies. The transducers consist of a passive metal cap structure, and a thin piezoelectric disc rigidly bonded to the inside. Extensive finite element modelling, and experimental 2D, time-resolved displacement measurements were done to characterise the transducers flexural properties, and to compare them to the analytical solutions of thin vibrating plates. Emphasis was put on characterising the passive layer of the unimorph structure, before bonding the piezoelectric element, to understand how the active element affects the behaviour of the flexing plate. A high power Nd:YAG laser was used to actuate the metal plate (non-contact), and the frequency content of the resulting displacement signal was analysed to identify the flexural modes. The non-axisymmetric modes, which are conventionally disregarded because of their unfavourable acoustic properties, were also taken into account. There was excellent agreement between the experimental results and the FE simulation data. There was good agreement with the analytical edge clamped plate model, but with some notable deviations, which have not previously been identified or commented upon. Specifically, the second axisymmetric mode is split into three separate modes, which is not explained by the traditional theory of plates. The analysis is similar to that of contemporary pMUT research, but with the proposed macroscopic dimensions and passive metal layer making the transducer industrially robust, cheap and easy to manufacture, and more suitable for a different range of applications where these aspects are of importance.**

I. Introduction

The field of air-coupled ultrasonics has received an increased interest over the years, as it has expanded into new areas of application, including wireless communication [1], contactless material characterisation [2], gas flow metering [3], [4] and robotics [5]. Each application has its own set of requirements, which has pushed the development of transducer technology. The perpetual problem of air-coupled transduction is the large acoustic impedance mismatch, between the transducer element (typically PZT) and the propagation medium, causing an inefficient power output and narrow operating bandwidth.

The classical solution is to gradually decrease the impedance along the path of propagation, by introducing one or more matching layers [6], often with a combined thickness of a quarter wavelength. In order to match the transducer impedance to air, low density, often porous, materials are needed [7]. This as well as the introduction of multiple boundaries that can cause failure by debonding, makes the transducer less robust and unsuitable for some industrial applications. For example, ultrasonic transducers used for flow measurements, often incorporate a metal cap that shields the piezoelectric and matching layer elements, but which inevitably causes signal loss and consequently the requirement of higher excitation voltages in these applications.

More recently piezocomposites [8], [9] and ferroelectrets [10] have successfully been used instead of traditional piezoceramics, because of their lower acoustic impedances. Piezocomposites will in general still require a matching layer to achieve acceptable efficiency, and ferroelectrets have high attenuation and are in themselves not very robust.

Electrostatic transducers, such as capacitative micromachined ultrasonic transducers (CMUTs) [11], [12], have been demonstrated to have excellent coupling to air, as well as an enhanced bandwidth. However, the requirements of a large bias voltage, as well as a thin flexible membrane as the radiating front face, can be problematic for some applications, including gas flow measurements, where intrinsic safety is highly critical.

Another solution is to use the flexural modes of a metal plate or membrane to produce ultrasound. Because the plate displaces the air by bending, its mechanical impedance is much lower than the acoustic impedance of the plate material [13]. Transducers built on this principle, known as flexural transducers [14]–[19], can produce large displacements for a relatively low excitation voltage. In such a device configuration, a piezoelectric disc can be bonded directly to the back of the plate, without matching layers, thus minimising the number of surface bonds that can fail over time. Also, by having a metal plate as the radiating front face, the transducer gains an inherent robustness, for which other transducers would suffer a signal loss. These types of ceramic-metal transducers, also known as unimorphs [20], bimorphs [21] or multimorphs depending on the number of active layers, are not only used for ultrasound transduction, but can be found in a variety of actuator applications, e.g. energy harvesting [22], where their vibrational and flexing properties are exploited.

Air-coupled flexural transducers are typically used for low power proximity measurements [23], e.g. in parking sensors, as well as for high power ultrasonics [24], [25]. Low frequency, typically 40 kHz or lower, flexural transducers are commercially available. However, many applications require higher

frequency signals, and the designs proposed in this paper allowed operating frequencies of $\sim$ 90 kHz and $\sim$ 150 kHz respectively.

Some initial results and analyses by the authors on flexural transducers, upon which this article extends, can be found in the conference proceedings [26], [27].

The frequency of the vibrations and hence of the ultrasonic wave, depends on the driving frequency of the electrical signal applied to the piezoelectric element, but large amplitude displacements are achieved by driving the system at its resonance frequencies. The resonance frequencies, i.e. the modal frequencies, of the system depend on the geometry of the passive layer and the piezoelectric disc, and are not significantly affected by the through thickness resonance modes of the piezoelectric element, which due to the small thickness are typically over an order of magnitude greater than the operational frequency of the flexural transducer.

Flexural transducers share many traits with the more recently developed piezoelectric micromachined ultrasonic transducers (pMUTs) [28], which combine the enhanced fluid coupling of flextensional vibrations of a plate with micro electromechanical systems (MEMS) technology. In essence, a pMUT is an array of miniaturised flexural transducers operating in the fundamental bending mode. They have demonstrated enhanced bandwidth and good fluid coupling, but lack the intrinsic robustness of the macro flexural transducer. Also, because of the microscopic nature of pMUTs, the manufacturing process is more complicated and expensive. An excellent article with experimental validation of theoretical calculations on the flexural properties of the single pMUT element is found in [29].

A. Theory of Vibrations in Plates

The equation describing the time dependent, normal displacement of a thin plate is a fourth order partial differential equation [30]:

$$D\nabla^4 w(\mathbf{x},t) + \rho\frac{\partial^2 w(\mathbf{x},t)}{\partial t^2} = 0, \tag{1}$$

where w is the normal displacement of the plate, ρ is the volume density and D is the rigidity, which is given by

$$D = \frac{Eh^3}{12(1-\nu^2)}, \tag{2}$$

where E is Young's modulus, h is the plate thickness and ν is Poisson's ratio. Solving (1) to find mode shapes $W_{m,n}$ gives

$$W_{m,n}(r,\theta) = \left(A_n I_n(\frac{\lambda_{m,n}}{a}r) + B_n J_n(\frac{\lambda_{m,n}}{a}r)\right)\cos(n\theta), \tag{3}$$

where A_n and B_n are constants determined by the boundary conditions, a is the plate radius, $\lambda_{m,n}$ is the mode constant for the (m,n) mode, which has m radial nodes (excluding the outer edge) and n nodal diameters. The frequency of a mode is given by

$$f_{m,n} = \frac{1}{2\pi}\left(\frac{\lambda_{m,n}}{a}\right)^2\sqrt{\frac{D}{\rho}}. \tag{4}$$

Fig. 1 illustrates the mode numbering convention used, which is also used in [30]. Some numerically calculated values of λ are given in Table I.

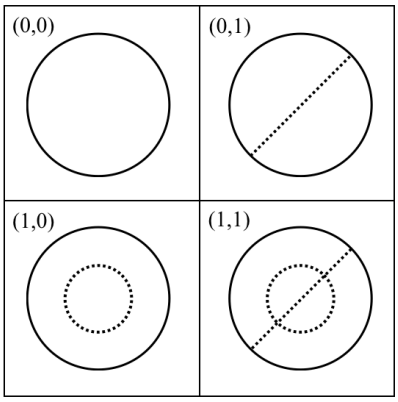

Fig. 1: Nodal lines of the four first modes of an edge clamped plate.

TABLE I: Numerically calculated values of the mode constant $\lambda_{m,n}$ of a clamped plate, from (3), for $m = 0,1,2$ and $n = 0,1,2$.

m \ n	0	1	2	3
0	3.19625	4.61085	5.90565	7.14355
1	6.30645	7.79925	9.19685	10.5366
2	9.43945	10.958	12.4022	13.795

II. Methods

The two transducer designs are schematically shown with labeled dimensions in Fig. 2. Two types of transducers were made, one from aluminium and one from titanium. The values of the dimensions for each type of transducer is given in Table II. Aluminium was chosen because it is easy to process, and titanium because it is the gold standard for durability and strength to weight ratio in industry. For similar reason stainless steel was also initially tested, but its material properties makes it less efficient for flexural transduction.

Finite element (FE) methods [33], using software package PZFlex (Weidlinger Associates Inc., USA), were used to simulate axisymmetric flexural transducers. The FE model was used to find the modal frequencies of the transducer as well as for looking at the mode shapes. The effects on mode frequencies due to small variations in dimensions of the passive layer were also studied.

Before the transducers were fully assembled the flexural properties of the passive layer (the metal cap) were studied, by measuring the transverse displacement of the front face. The transducers were excited thermoelastically [34] by a 10 ns

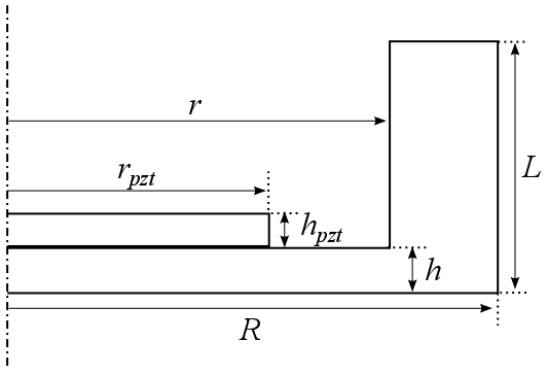

Fig. 2: Axisymmetric schematic diagram of the transducer, with labeled dimensions.

TABLE II: Dimensions of the transducers in mm.

Dim. \ Trans.	Al	Ti
r	4.5	5.2
R	5.5	6.0
h	0.5	0.25
L	5.0	4.0
r_{pzt}	3.2	1.5
h_{pzt}	0.5	0.25

laser pulse, from an Nd:YAG laser, and the displacement was measured at a point of the front face with a two wave mixer laser interferometer [35]. The displacement was measured both at the centre of the front face and off-centre, in order to separate the axisymmetric modes from the non-axisymmetric, as the non-axisymmetric modes have zero displacement along a diameter.

The aluminium caps were also excited electrodynamically [27] (non-contact), and the displacement signal of the whole radiating face measured, using a Polytec (OFV-5000) laser vibrometer and an xy-stage. Signal processing was used to filter out the vibrations from individual modes, in order to identify and characterise them.

The piezoelectric discs were attached to the back of the caps with hard-set conductive epoxy. A function generator (Tektronix AFG 3502C) was used to both generate broadband pulses and continuous sinusoidal excitation at the modal frequencies of the transducers. The assembled transducers were tested in terms of front face displacement and acoustic pressure.

III. Results

The frequency spectra from the unloaded transducer caps are shown in Fig. 4. The fundamental mode (0,0) is clearly dominant for the aluminium cap, which has higher mode

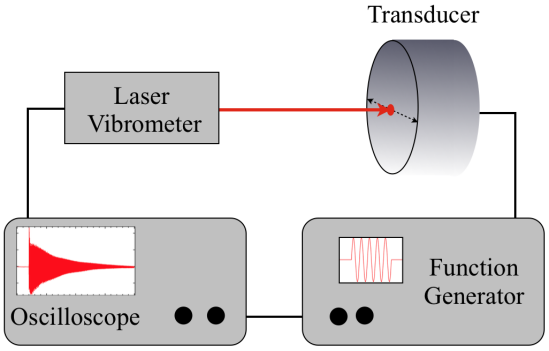

Fig. 3: Schematic diagram of the setup used to measure the front face displacement of a flexural transducer with a laser vibrometer.

frequencies compared to the titanium cap. However, higher modes are still visible in the spectra, and are more prominent in the simulated data. One interesting feature is the three closely spaced peaks in Fig. 4a, which were present in both the simulated and experimental data, but does not emerge from the theoretical model. The middle peak at $\sim$ 180 kHz, is roughly

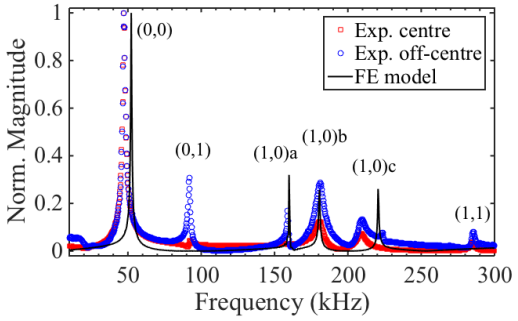

(a) Al cap

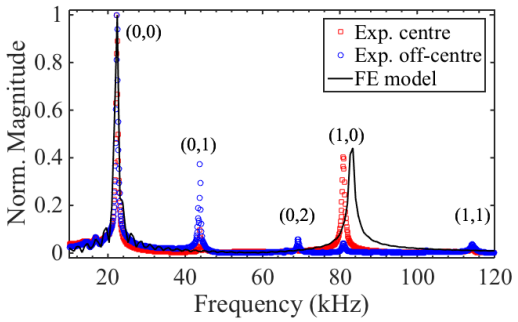

(b) Ti cap

Fig. 4: Frequency spectra from the passive layers of the unimorph, excited by non-contact methods. Non-axisymmetric modes can be identified as those that are not present in the FE data, and have smaller magnitude at the centre of the cap.

were the (1,0) mode is expected from (5). By looking at the mode shapes from the FE model, in Fig. 5, it is seen that all three frequencies correspond to modes with one nodal radius,

i.e. the (1,0) mode. Hence, these modes are referred to as (1,0)a, (1,0)b and (1,0)c respectively in order of increasing frequency. The shapes Fig. 5 shows that the main difference between these modes is the displacement close to the edge. Because the edges of the cap are not strictly clamped, the boundary of the outer radius of the plate is not well defined. (1,0)a behaves like a vibrating plate with a radius close to that of the outer radius ($R = 5.5$ mm) of the cap, and (1,0)c as a plate with radius close to the inner radius ($r = 4.5$ mm) of the cap. And as expected (1,0)b has shape that suggests a plate with a radius between the inner and outer radius of the cap. For the fundamental mode, using (5) and $\lambda_{0,0} = 3.2$ we get $f_{0,0}(a = R) = 42$ kHz and $f_{0,0}(a = r) = 62$ kHz, with the experimental value, from the peak in Fig. 4a, in between these two values at 50 kHz. In general it was found for a measured mode frequency $f^{exp}_{m,n}$

$$f_{m,n}(a = R) < f^{exp}_{m,n} < f_{m,n}(a = r). \quad (5)$$

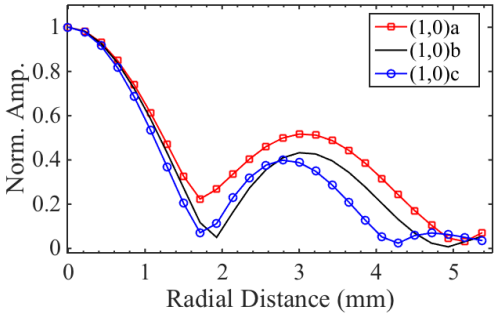

Fig. 5: The split (1,0) mode shapes of the Al cap, from the FE model.

Looking at the experimental data from the displacement scan in Fig. 6, the split mode shapes become more complicated. The same trend in the outer radius as that observed in the FE model is seen, but the relative amplitude of the outer antinode to the centre antinode also changes. The spread of the experimental data for a given value of r indicates how axisymmetric the mode is. In the limit of a perfectly axisymmetric mode the spread would be zero along the mode shape. Hence, it is seen that both (1,0)a and (1,0)c are picking up contributions from non-axisymmetric modes. Since the FE model is inherently axisymmetric this could not be observed in the simulated data. A reasonable explanation for this spread comes from the proximity of (1,0)a to the (0,2) mode, and the proximity of (1,0)c to the (0,3) mode, as seen in Table I.

Fig. 7 shows the experimentally observed mode shapes of (0,0), (0,1), (1,0)b and (1,1) in 3D of the Al cap. Being able to visualise the actual movement of the front face gives insight into the flexural behaviour of the metal cap, and gives final confirmation as to the identity of the modes.

To see how the frequency of a mode changes with small variations in the dimensions of the cap, the inner radius

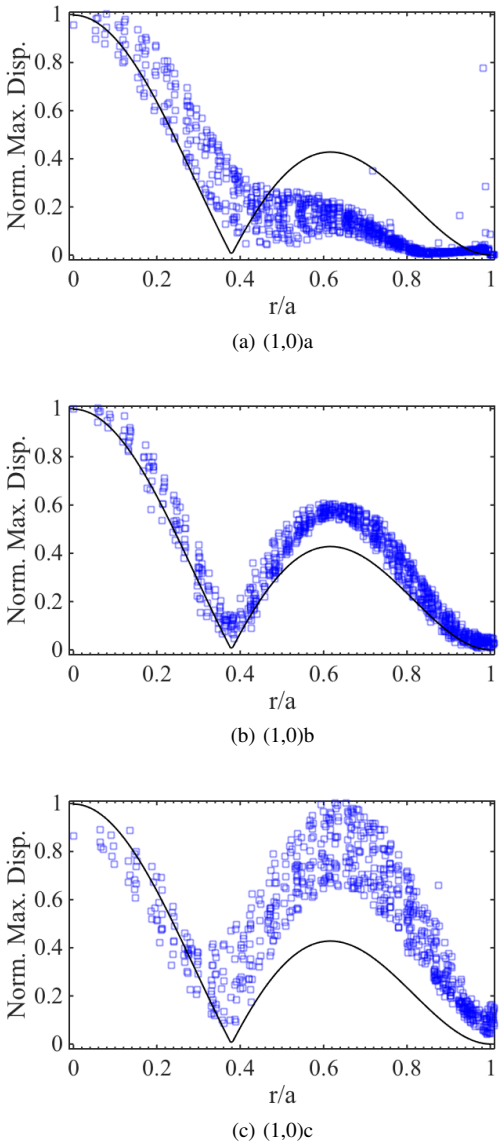

(a) (1,0)a

(b) (1,0)b

(c) (1,0)c

Fig. 6: Experimental, normalised, mode shapes of the split (1,0) mode of the Al cap as a function of dimensionless radius, compared with the theoretical mode shape from (3). (a) mode (1,0)a at 160 kHz with $a = 5.5$ mm, (b) mode (1,0)b at 180 kHz with $a = 5.0$ mm, and (c) mode (1,0)c at 210 kHz with $a = 4.5$ mm.

and thickness of the front face of the cap in the FE model were varied and the fundamental mode frequency recorded. The results are plotted in Fig. 8. As expected the frequency decreases with an increasing radius and increases with an increasing thickness, as described by (5). The results are in good agreement with the results from the theoretical model of an edge clamped plate.

After the transducers were assembled, with the piezoelectric disc bonded to the back of the cap (as in Fig. 2) the frequency spectra of each cap was analysed again. Fig. 9 and Fig. 10

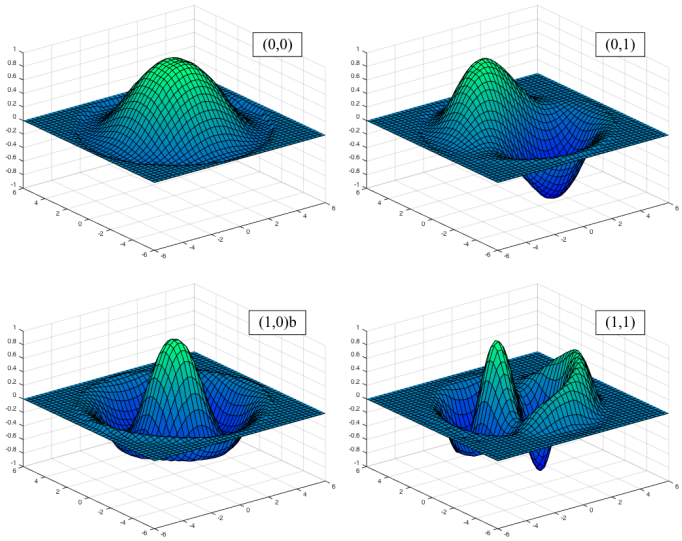

Fig. 7: (Animated online) experimentally observed modes of the Al cap, corresponding to the peaks in the frequency spectra in Fig. 4a. The amplitude of each individual mode has been normalised, but the relative frequencies of the modes are accurately represented in the animation.

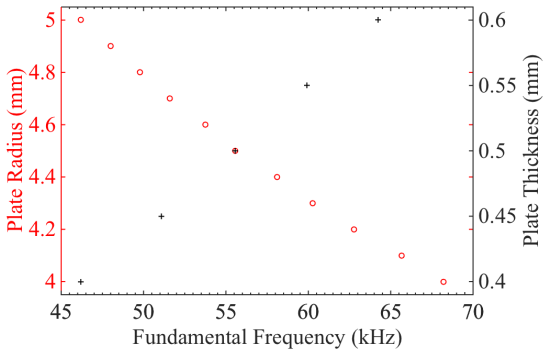

Fig. 8: The fundamental frequency of the transducer as the thickness is varied with a fixed inner radius of 4.5 mm (+), and the as the radius is varied with a fixed thickness of 0.5 mm (○).

shows the frequency spectra from for the Al and Ti transducers respectively. The spectra from the Al transducer has notably changed in terms of relative amplitude of the modes, e.g. the (1,0)c mode has greater amplitude than the fundamental mode. However, this effect could be due to the excitation signal, rather than the loading of the active element. Also, there are small shifts in the frequency of some modes, e.g. (1,0)a has been shifted down by approximately 10 kHz.

The far-field beam profile of (1,0)a, measured with an acoustic microphone, is shown in Fig. 11. The large displacement of the outer antinode of the plate gives rise to large side lobes, which can be problematic in some applications.

Similarly for the Ti transducer, the higher modes became

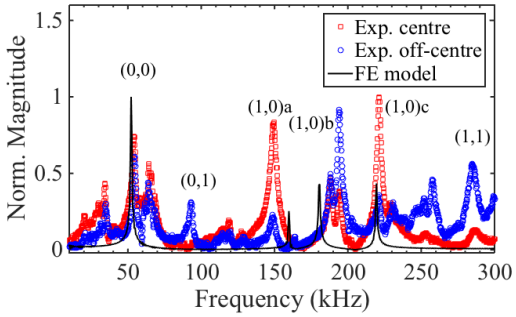

Fig. 9: Frequency spectrum from the piezoelectrically actuated Al flexural transducer, excited by a broadband pulse.

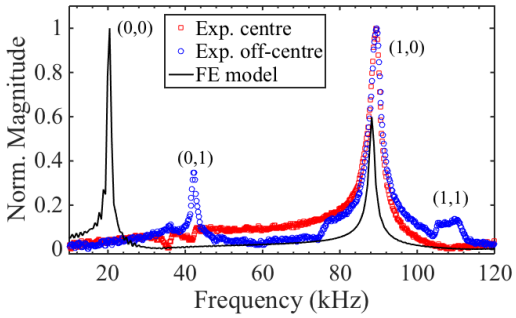

Fig. 10: Frequency spectrum from the piezoelectrically actuated Ti flexural transducer, excited by a broadband pulse.

more prevalent after attaching the piezoelectric disc. There is however a significant difference from the simulation data. In the FE model the fundamental mode is still dominant, whereas it is almost completely absent in the experimental results. This surprising result was verified in another five transducers. There is also a frequency shift of the (1,0) mode of $\sim$ 10 kHz, which was expected from the additional rigidity and effective thickness introduced by the active layer.

One important characteristic of a flexural transducer is the

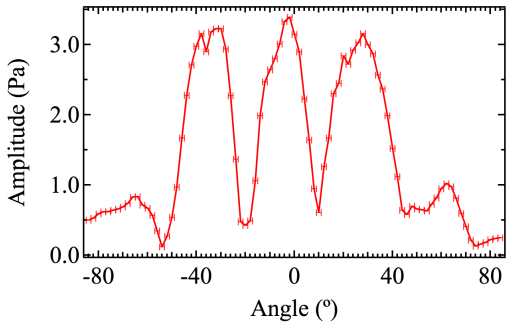

Fig. 11: Far-field beam profile of the transducer operating in the (1,0)a mode, at 150 kHz, taken at a distance of 20 cm from the front face.

deflection of the front face for a given input, and increases with improved electromechanical coupling. The frequency and axisymmetric shape of the (1,0) mode of the Ti transducer make it suitable for ultrasonic transduction. Fig. 12 shows the front face displacement (animated online) and frequency data from the Ti transducer when excited by 2.5 V amplitude, 3 cycle, sinusoidal signal, at 89 kHz. The addition of the piezoelectric disc caused the shape profile to flatten at the central antinode, and the outline of the disc can be roughly made out. This also causes the relative amplitude of the outer antinode to increase in comparison, making the shape deviate from (3).

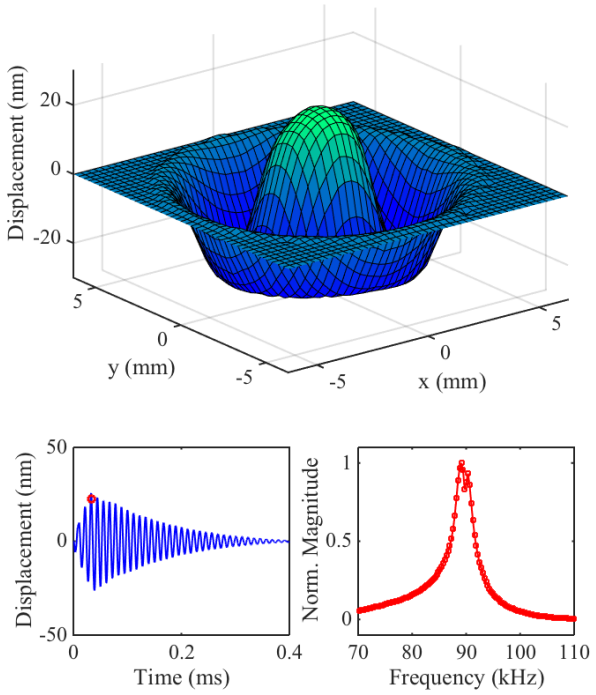

Fig. 12: (Animated online) instantaneous absolute displacement across the transducer front face, centre point displacement, and its frequency content of the Ti transducer, when excited by a gated, 89 kHz, sine signal.

IV. Conclusions

The flexural transducers investigated use modes similar to those of a circular edge clamped plate. FE analysis shows how the individual modes predicted by the analytical theory split as a result of the boundary conditions of the cap geometry. The frequencies predicted by the theory are comparable to those given by the FE model, and those measured experimentally. For a flexural transducer cap design, which has an inner and outer radius, the measured mode frequency lies within the limits of an edge clamped plate with radius $a = r$ (upper limit) and $a = R$ (lower limit). Significant contribution from the non-axisymmetric modes were found in the split modes (1,0)a and (1,0)c of the aluminium transducer, which can be explained by the proximity of the (1,0) mode to the (0,2) and (0,3) modes. These are factors that need to be considered when designing a flexural transducer, and which cannot be directly predicted from the analytical theory.

It was also seen that the flexural properties of the transducer were determined and could be predicted from the passive layer alone. This is important in the manufacturing stage, as it allows for quality control, e.g. in terms of frequency matching, before assembling the transducer.

References

[1] C. Li, D.A. Hutchins and R.J. Green, "Short-Range Ultrasonic Communications in Air Using Quadrature Modulation," IEEE Trans. Ultrason. Ferroelectr. Freq. Control **56**, 2060–2072 (2009).

[2] D.E. Chimenti, "Review of Air-Coupled Ultrasonic Materials Characterization," Ultrasonics **54**, 1804–1816 (2014).

[3] H.J. Dane, "Ultrasonic Measurement of Unsteady Gas Flow," Flow Meas. Instrum. **8**, 183–190 (1997).

[4] I.J. O'Sullivan and W.M.D. Wright, "Ultrasonic Measurement of Gas Flow Using Electrostatic Transducers," Ultrasonics **40**, 407–411 (2002).

[5] J. Borenstein and Y. Koren, "Obstacle Avoidance with Ultrasonic Sensors," IEEE J. Robotics Automat. **4**, 213–218 (1988).

[6] A.J. Muholland, S.N. Ramadas, R.L. O'Leary, A.C.S. Parr and G. Hayward, "Enhancing the Performance of Piezoelectric Ultrasound Transducers by the Use of Multiple Matching Layers," IMA J. Appl. Math. **73**, 936–949 (2008).

[7] T.E. Gómez Álvarez-Arenas, "Acoustic Impedance Matching of Piezoelectric Transducers to the Air," IEEE Trans. Ultrason. Ferroelectr. Freq. Control **51**, 624–633 (2004).

[8] M.I. Haller and B.T. Khuri-Yakub, "Micromachined 1-3 Composites for Ultrasonic Air Transduction," Rev. Sci. Instrum. **65**, 2095–2098 (1994).

[9] G. Hayward and A. Gachagan, "An Evaluation of 1-3 Connectivity Composite Transducers for Air-Coupled Ultrasonic Applications," J. Acoust. Soc. Am. **99**, 2148–2157 (1996).

[10] R. Kressman, "New Piezoelectric Polymer for Air-Borne and Water-Borne Sound Transducers," J. Acoust. Soc. Am. **109**, 1412–1416 (2001).

[11] D.W. Schindel and D.A. Hutchins, "Applications of Micromachined Capacitance Transducers in Air-Coupled Ultrasonics and Nondestructive Evaluation," IEEE Trans. Ultrason. Ferr. Freq. Cont. **42**, 51–58 (1995).

[12] I. Ladabaum, X.C. Jin, H.T. Soh, A. Atalar and B.T. Khuri-Yakub, "Surface Micromachined Capacitive Ultrasonic Transducers," IEEE Trans. Ultrason. Ferroelectr. Freq. Control **45**, 678–690 (1998).

[13] M. Toda, "New Type of Matching Layer for Air-Coupled Ultrasonic Transducers," IEEE Trans. Ultrason. Ferr. Freq. Cont. **49**, 972–979 (2002).

[14] C.P. Germano, "Flexure Mode Piezoelectric Transducers," IEEE Trans. Audio Electroacoust. **AU19**, 6–12 (1971).

[15] W.J. Denkmann, R.E. Nickell and D.C. Stickler, "Analysis of Structural-Acoustic Interactions in Metal-Ceramic Transducers," IEEE Trans. Audio Electroacoust. **AU21**, 317–324 (1973).

[16] J.F. Tressler, W. Cao, K. Uchino and R.E. Newnham, "Finite Element Analysis of the Cymbal-Type Flextensional Transducer," IEEE Trans. Ultrason. Ferr. Freq. Cont. **45**, 1363–1369 (1998).

[17] X. Hu, L. Li, X. Chu and Z. Gui, "The Resonance Vibration Properties of a Bimorph Flexural Piezoelectric Ultrasonic Transducer for Distance Measurement," Mater. Sci. Eng. **B99**, 316–320 (2002).

[18] H. Yihua and H. Wenbin, "Research on the Displacement Function and Equivalent Circuit of Circular Flexural Vibration Mode Piezoelectric Ceramic Composite Transducers," IEEE Trans. Ultrason. Ferr. Freq. Cont. **60**, 218–234 (2013).

[19] H. Xiping, Z. Ting and P. Xiaojuan, "Analytical and Experimental Investigation on Thick Plates in Flexural Vibration," Acta Acust. United Ac. **100**, 411–417 (2014).

[20] J. Yang, H. Zhou and S. Dong, "Analysis of Plate Piezoelectric Unimorphs," IEEE Trans. Ultrason. Ferr. Freq. Cont. **53**, 456–462 (2006).

[21] J.G. Smits, S.I. Dalke and T.K. Cooney, "The Constituent Equations of Piezoelectric Bimorphs," Sens. and Actuators, A **28**, 41–61 (1991).

[22] C. Kim and J. Lee, "Topology Optimum Design of Unimorph Piezoelectric Cantilevered Mandolin Plates as A Vibrating Electric Harvester," J. Mech. Sci. Technol. **28**, 4131–4138 (2014).

[23] W. Manthey, N. Kroemer and V. Magor, "Ultrasonic Transducers and Transducer Arrays for Applications in Air," Meas. Sci. Technol. **3**, 249–261 (1992).
[24] A. Barone and J.A. Gallego-Juàrez, "Flexural Vibrating Free-Edge Plates with Stepped Thickness for generating High Directional Ultrasonic Radiation," J. Acoust. Soc. Am. **51**, 953–959 (1972).
[25] E. Riera-Franco de Sarabia, J.A. Gallego-Juárez, G. Rodríguez-Corral, L. Elvira-Segura and I. González-Gómez, "Application of High-Power Ultrasound to Enhance Fluid/Solid Particle Separation Process," Ultrasonics **38**, 642–646 (2000).
[26] T.J.R. Eriksson, S.M. Dixon and S.N. Ramadas, "Flexural Mode Metal Cap Transducer Design for Specific Air Coupled Ultrasound Generation," in: 2013 IEEE International Ultrasonics Symposium.
[27] T.J.R. Eriksson, M. Laws, S.M. Dixon and S.N. Ramadas, "Air-Coupled Flexural Electrodynamic Transducers," in: 2014 IEEE International Ultrasonics Symposium.
[28] F. Akasheh, T. Myers, J.D. Fraser, S. Bose and A. Bandyopadhyay, "Development of Piezoelectric Micromachined Ultrasonic Transducers," Sens. and Actuators, A **111**, 257–287 (2004).
[29] K. Smyth and S.-G. Kim, "Experiment and Simulation Validated Analytical Equivalent Circuit Model for Piezoelectric Micromachined Ultrasonic Transducers," IEEE Trans. Ultrason. Ferr. Freq. Cont. **62**, 744–765 (2015).
[30] A.W. Leissa, *Vibration of Plates* (U.S. Government Press, Washington, 1969), pp. 1–8.
[31] W. Soedel, *Vibrations of Shells and Plates* (Marcel Dekker inc., New York, third revised edition, 2004). pp. 102–106.
[32] G. Arfken, H. Weber and F. Harris, *Mathematical Methods for Physicists: A Comprehensive Guide* (Elsevier Academic, Oxford, Seventh Edition, 2012), pp. 643–713.
[33] L.W. Schmerr, *Fundamentals of Ultrasonic Nondestructive Evaluation: A Modeling Approach* (Plenum Press, New York, 1998), pp. 1–559.
[34] C.B. Scruby and L.E. Drain, *Laser Ultrasonics: Techniques and Applications* (Adam Hilger, Bristol, 1990).
[35] M.B. Klein, G.D. Bacher, A. Grunnet-Jepsen, D. Wright adn W.E. Moerner, "Homodyme Detection of Ultrasonic Surface Displacements using Two-Wave Mixing in Photorefractive Polymers," Opt. Commun. **162**, 79–84 (1999).